Title	Pressure-stabilized tin selenide phase with an unexpected stoichiometry and a predicted superconducting state at low temperatures
Author(s)	YU, H; Lao, W; Wang, L; Li, K; Chen, Y
Citation	Physical Review Letters, 2017, v. 118, p. 137002:1-5
Issued Date	2017
URL	http://hdl.handle.net/10722/243124
Rights	Physical Review Letters. Copyright © American Physical Society.; This work is licensed under a Creative Commons Attribution-NonCommercial-NoDerivatives 4.0 International License.

Pressure-Stabilized Tin Selenide Phase with an Unexpected Stoichiometry and a Predicted Superconducting State at Low Temperatures

Hulei Yu,[1] Wenxin Lao,[1] Lijuan Wang,[2] Kuo Li,[2,*] and Yue Chen[1,†]
[1]Department of Mechanical Engineering, The University of Hong Kong, Pokfulam Road, Hong Kong SAR, China
[2]Center for High Pressure Science and Technology Advanced Research, 10 Dongbeiwang West Road, Haidian, Beijing 100094, China
(Received 14 October 2016; revised manuscript received 17 February 2017; published 28 March 2017)

Tin-selenium binary compounds are important semiconductors that have attracted much interest for thermoelectric and photovoltaic applications. As tin has a +2 or +4 oxidation state and selenium has an oxidation number of −2, only SnSe and $SnSe_2$ have been observed. In this work, we show that the chemical bonding between tin and selenium becomes counterintuitive under pressures. Combining evolutionary algorithms and density functional theory, a novel cubic tin-selenium compound with an unexpected stoichiometry 3:4 has been predicted and further synthesized in laser-heated diamond anvil cell experiments. Different from the conventional SnSe and $SnSe_2$ semiconductors, Sn_3Se_4 is predicted to be metallic and exhibit a superconducting transition at low temperatures. Based on electron density and Bader charge analysis, we show that Sn_3Se_4 has a mixed nature of chemical bonds. The successful synthesis of Sn_3Se_4 paves the way for the discovery of other IV-VI compounds with nonconventional stoichiometries and novel properties.

DOI: 10.1103/PhysRevLett.118.137002

Tin-selenium compounds are important semiconductors and widely applied in photovoltaics, thermoelectrics, and memory-switching devices [1–3]. As tin has an oxidation state of +2 or +4 and selenium has a −2 oxidation number, the conventional binary compounds observed in the tin-selenium system are tin selenide (SnSe) and tin diselenide ($SnSe_2$), which represent the typical stoichiometries in the IV–VI group. SnSe is a narrow band gap semiconductor with an unprecedented thermoelectric efficiency [4,5]. It was shown that laminar SnSe ($B16$-type structure in the *Pnma* space group) undergoes a pressure-induced structural phase transition to the $B33$ structure (*Cmcm* space group) at about 10.5 GPa [6]. Under further compression, SnSe transforms into the $B2$ structure ($Pm\bar{3}m$ space group) and this phase was found to exhibit a superconducting transition at low temperatures above 58 GPa [7]. $SnSe_2$ is also a layered semiconductor with a hexagonal CdI_2-type crystal structure ($P\bar{3}m1$ space group) [8]. From x-ray diffraction (XRD), it was found that $SnSe_2$, which is important for photoelectric applications [9], shows a second polytype with a space group of $R\bar{3}m$ [10]. On the other hand, the compound Sn_2Se_3 has a controversial stoichiometry; it was argued that this compound is simply a superposition of SnSe and $SnSe_2$ [11].

Novel phases and compounds may be synthesized under high pressures [12,13]. Theory-assisted material discovery based on the *ab initio* evolutionary approach has been shown to be extremely effective [14–17]. Calcium carbides were investigated up to 100 GPa from first principles using the variable-composition evolutionary approach; two new compounds, Ca_2C and Ca_2C_3, were predicted and successfully synthesized [18]. In the Zr-B binary system, Zr_3B_2 and Zr_2B_3 were predicted to be metastable below 50 GPa from the evolutionary approach [19]. Zhang *et al.* predicted some unexpected stable stoichiometries in the sodium-chlorine system under high pressures [20]. Drozdov *et al.* recently observed a record high superconducting transition temperature in the sulfur-hydrogen system [21], in which the crystal structure of the new phase was firstly predicted from theory [22,23].

Combining density functional theory (DFT) and evolutionary algorithms [24,28], we carried out variable-composition structural searches in the Sn-Se system at pressures up to 40 GPa. A maximum number of 14 atoms is allowed in a unit cell in our calculations. High pressure-high temperature experiments were performed to synthesize the predicted new compounds using commercial selenium powder (Alfa Aesar, 99.999%) and tin powder (Alfa Aesar, 99.995%) as reactants. A mixture of Sn and Se powder with a molar ratio of 3:4 was loaded into a diamond anvil cell equipped with 400 μm culet diamonds and a stainless steel gasket. MgO was also loaded on the diamonds as the thermal isolator. The reactant mixture was compressed to 16.4 GPa and heated up to 1225 K using the on-line double-sided laser heating system at 16-IDB, Advanced Photon Source, and *in situ* powder x-ray diffraction was carried out simultaneously. The pressure was measured using the ruby fluorescence method [30]. The XRD data were collected using a PILATUS 1M detector and integrated using Dioptas [31].

It is seen, from the convex hulls in Fig. 1, that there are two stable compounds, SnSe and $SnSe_2$, that are energetically preferable at low pressures. As expected, SnSe goes through a phase transition from the *Pnma* structure through *Cmcm* to a higher symmetry $B2$ structure with increasing pressure.

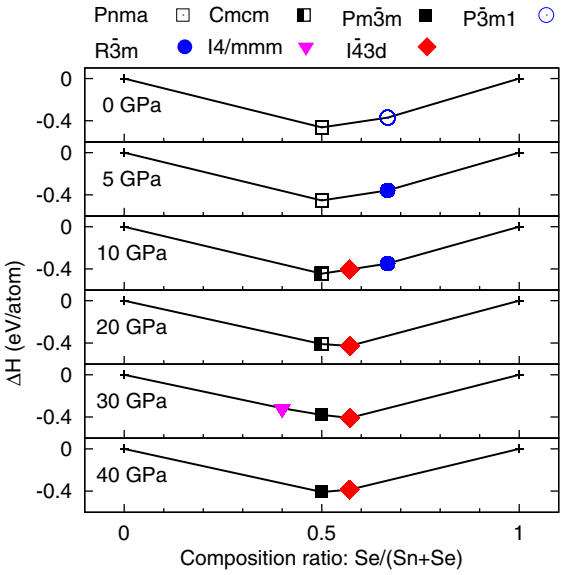

FIG. 1. Enthalpies of formation of the predicted stable compounds in the Sn-Se binary system. Solid lines represent the convex hulls at different hydrostatic pressures.

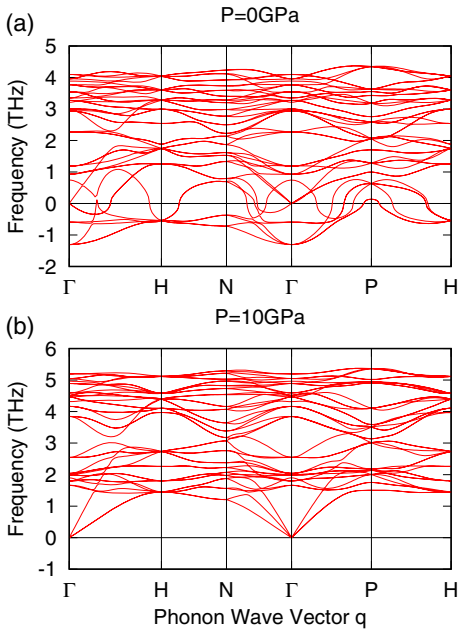

FIG. 2. Phonon dispersions of the predicted Sn_3Se_4 compound at hydrostatic pressures of 0 GPa (a) and 10 GPa (b). The negative values represent imaginary phonon frequencies.

The high-pressure crystal structures and the corresponding phase transition pressures are in good agreement with experimental observations [6,7], indicating the reliability of our calculations. $SnSe_2$ has a CdI_2-type structure with a space group of $P\bar{3}m1$ at 0 GPa, and it transforms into the $R\bar{3}m$ space group at 5 GPa. These two competing phases of $SnSe_2$ have very similar enthalpies at 0 GPa; e.g., $R\bar{3}m$ is only ~3.5 meV/atom higher in enthalpy than $P\bar{3}m1$, which may explain the experimental observations of different $SnSe_2$ polytypes. It is also noted that the convex hull at 20 GPa does not contain the 1:2 stoichiometry, indicating that $SnSe_2$ becomes unstable and decomposes at high pressures. On the other hand, a new compound with an unexpected stoichiometry, 3:4, in the $I\bar{4}3d$ space group is predicted to be energetically stable at 10 GPa. It is likely that $SnSe_2$ spontaneously decomposes into Sn_3Se_4 and Se at high pressures. As can be seen from the convex hulls, Sn_3Se_4 is energetically preferable up to the highest pressure considered in this work. The large pressure range where Sn_3Se_4 is energetically preferable makes it possible to synthesize the compound. Unlike the layered crystal structures of SnSe and $SnSe_2$, Sn_3Se_4 has a more densely packed Th_3P_4-type crystal structure, which was mostly observed in compounds formed between rare earth and group IV, group V, or group VI elements [32], or between transition metals (group IVB) and group V elements [33]. For the main-group binary compounds, only IV–V compounds were reported to have the Th_3P_4-type structure at high pressures [34]. Materials having this type of crystal structure were found to demonstrate great hardness, thermoelectricity, ferromagnetism, or superconductivity [32,35,36]. In addition, a marginally stable Sn_3Se_2 in the $I4/mmm$ space group is observed at 30 GPa on the convex hull. However, the narrow pressure range where this compound exists makes it difficult to synthesize.

In addition to the energetics, we have studied the dynamical stability of Sn_3Se_4 under high pressures [37]. Phonon dispersions have been calculated from first principles at $T = 0$ K, as shown in Fig. 2. It is seen that Sn_3Se_4 is dynamically unstable at 0 GPa due to the existence of large imaginary phonon frequencies. With increasing pressure, it is seen from Fig. 2(b) that the imaginary phonon modes are hardened, and the system becomes dynamically stable at 10 GPa. Based on the enthalpy and phonon calculations, it is predicted that Sn_3Se_4 in the $I\bar{4}3d$ space group is energetically and dynamically stable at pressures above 10 GPa.

To verify our prediction on the new compound, we performed corresponding high-pressure experiments. The synchrotron XRD patterns at approximately 16.4 GPa and 1225 K with Le Bail fitting are shown in Fig. 3. The wavelength of the incident x ray is 0.4066 Å. The masked peaks (in gray) are from the thermal insulator MgO. It is seen that the predicted Sn_3Se_4 phase can be clearly identified from the XRD patterns. The nonfitted peaks in the XRD patterns may be attributed to the formation of unidentified metastable phases in the experiment. The refined lattice parameter from the XRD data is $a = 8.36$ Å and the space group is $I\bar{4}3d$. These experimental results are in excellent agreement with our calculations; the theoretical lattice parameter is 8.3 Å at 16 GPa and 0 K. The Sn_3Se_4 phase still exists when the system is recovered to room temperature at about 16.4 GPa, whereas it becomes unstable and decomposes when the pressure is released. The experiment is consistent with our phonon calculations, where

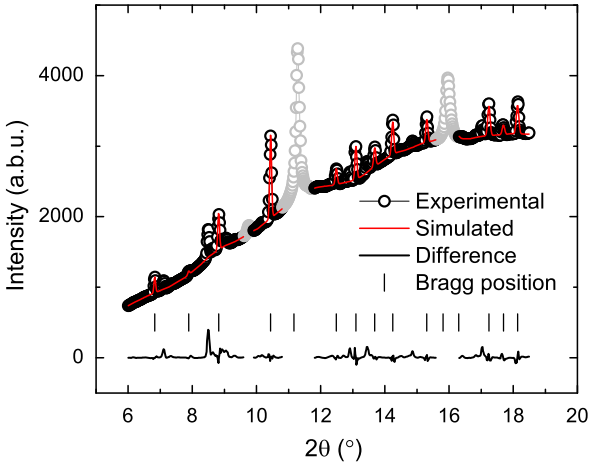

FIG. 3. Le Bail fitting plot of *in situ* XRD patterns of Sn_3Se_4 under 16.4 GPa and 1225 K. The experimental and simulated data are shown in black circles and red solid curves, respectively; their differences are shown in black solid curves and the Bragg positions are indicated by vertical bars. The peaks of MgO, the thermal isolator, are masked and shown in gray circles.

the imaginary phonon frequency of Sn_3Se_4 indicates a dynamical instability at ambient condition.

After the successful synthesis of Sn_3Se_4, we have further calculated its electronic band structure and density of states (DOS) using the modified Becke-Johnson method [39], which gives a more accurate band gap for SnSe [40]. As shown in Fig. 4(a), the band gap of SnSe is found to disappear at 10 GPa; a small overlap between the valence band maximum and the conduction band minimum is observed. The pseudogap at Fermi level indicates that SnSe exhibits a semimetallic behavior at 10 GPa, in agreement with a previous study [41]. From the projected band structure and DOS, it is found that the electronic states below Fermi level are mainly contributed by the Se $4p$ and Sn $5s$ orbitals; above Fermi level, the main contribution comes from the Sn $5p$ orbitals. For the new Sn_3Se_4 compound [see Fig. 4(b)], a large DOS is observed at Fermi level, corresponding to a metallic state. In the vicinity of the Fermi level, a majority of the electronic states originate from the Se $4p$ and Sn $5s$ orbitals. From the electronic structures of $SnSe_2$ [see Fig. 4(c)], it is interesting that a band gap opens up at Fermi level, suggesting that $SnSe_2$ is a semiconductor at 10 GPa with an indirect band gap of about 0.41 eV. The conduction band minimum is located in the F-P_1 path, and the valence band maximum is in the Z-Γ path. The bottom of the conduction bands mainly contain the Se $4p$ and Sn $5s$ states, showing significant s-p hybridizations; the top of the valance bands are largely the Se $4p$ states.

At high pressures above 58 GPa, SnSe was found to become a superconductor at temperatures below 4.5 K [7]. Comparing to SnSe, Sn_3Se_4 has a much lower metallization pressure, suggesting a potential superconductive transition at lower pressures. Based on the electron-phonon coupling

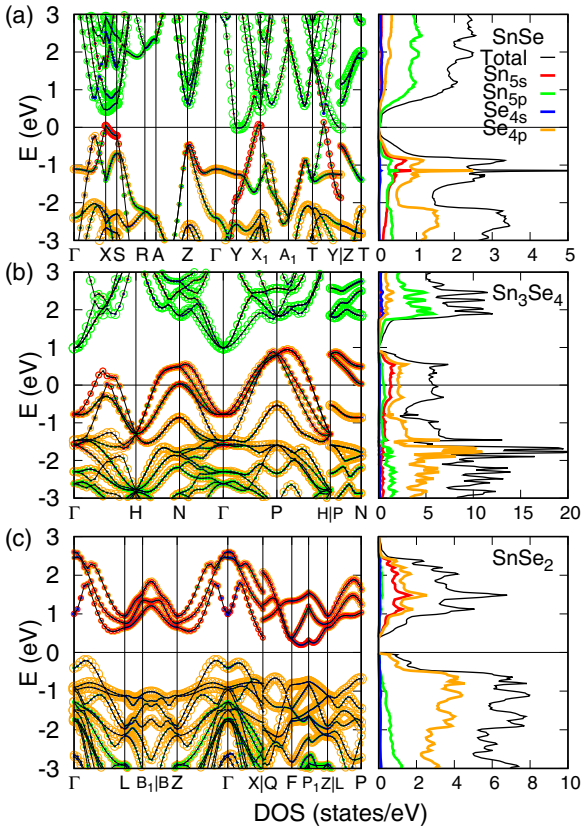

FIG. 4. Projected electronic band structures along high symmetry paths (left) and projected DOS (right) of SnSe (a), Sn_3Se_4 (b), and $SnSe_2$ (c), at 10 GPa. Fermi level is located at 0 eV. Different circle sizes correspond to the projected weights of different orbitals.

calculations, we have obtained the Eliashberg function at 10 GPa (see Fig. S1 in the Supplemental Material) [42]. Using the Allen-Dynes equation with typical values of the Coulomb pseudopotential μ^* in between 0.1 and 0.14, the superconducting transition temperature of Sn_3Se_4 is predicted to be in the range of 3.3–4.7 K at 10 GPa. Although the predicted T_c value needs further experimental verifications, the unexpected stoichiometry of Sn_3Se_4 results in a superconducting state at a much lower pressure than previously believed for the Sn-Se binary system.

From the charge density shown in Fig. 5, it is seen that electrons tend to move away from Sn atoms and concentrate around Se atoms, which is consistent with their oxidation states. It is also seen that the charge distributions are obviously directional. Therefore, the chemical bonds in these compounds are expected to exhibit a mixed ionic and covalent character. Because of the layered crystal structures of SnSe and $SnSe_2$, strong chemical bonds exist in the inner layer directions. In SnSe, all of the Sn atoms or Se atoms are in equivalent lattice sites. Each Sn atom is coordinated by one nearest neighbor Se atom ($d_1 = 2.7$ Å) and four next-nearest neighbor Se atoms ($d_2 = 2.9$ Å). Although d_1 and d_2 are rather similar, the charge density distributions

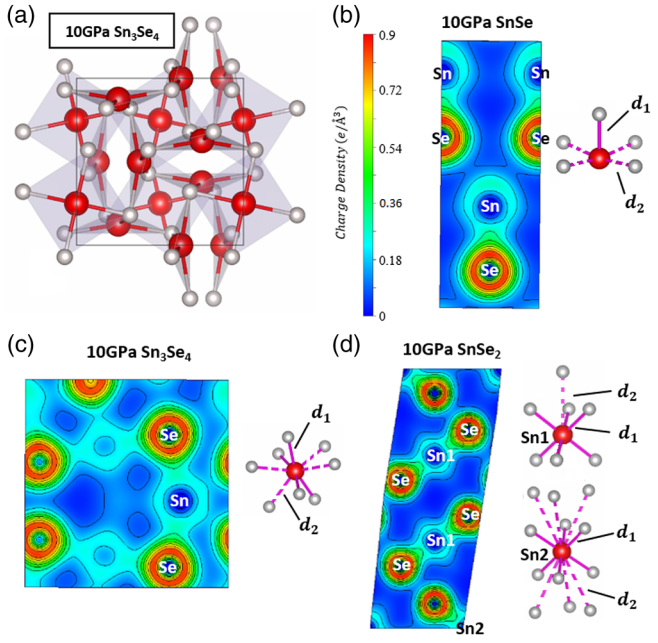

FIG. 5. (a) The conventional unit cell of Sn_3Se_4; red and grey spheres represent the Sn and Se atoms, respectively. Charge density distributions in SnSe (b), Sn_3Se_4 (c), and $SnSe_2$ (d) at 10 GPa; the corresponding coordination polyhedra are also given.

between the nearest and the next-nearest neighbors are significantly different. There are two nonequivalent Sn lattice sites and three nonequivalent Se lattice sites in $SnSe_2$. Different Sn sites have the same amounts of nearest neighbor Se atoms ($d_1 = 2.7$ Å) but different numbers of next-nearest neighbor Se atoms ($d_2 > 4.0$ Å). As the next-nearest neighbor Se atoms are relatively far away, nonequivalent Sn atoms show similar electron density distributions. For the newly discovered Sn_3Se_4, all Sn or Se atoms are equivalent. Each Sn atom has four nearest neighbor ($d_1 = 2.8$ Å) and four next-nearest neighbor ($d_2 = 3.1$ Å) Se atoms. It is noted that the charge density in the interstitial sites of Sn_3Se_4 is significantly higher than those in SnSe and $SnSe_2$. A more delocalized electron distribution in Sn_3Se_4 is consistent with its metallic behavior.

As Sn atoms exhibit oxidation states of +2 or +4, and Se atoms have a −2 oxidational number, the existence of SnSe and $SnSe_2$ is expected; nonetheless, the formation of Sn_3Se_4 is counterintuitive. Bader charge analysis [46] has been performed to further investigate the charge transfer in these compounds. It is seen from Table I that the number of electrons which each Sn atom donates to Se increases from SnSe through Sn_3Se_4 to $SnSe_2$. On the other hand, due to the increasing Se atomic percentage, the number of electrons which each Se atom accepts decreases. The electron transfers given by Bader charge analysis are significantly smaller than the standard oxidation numbers, which may be related to the mixed ionic and covalent bond characters as discussed in SnSe [47], $Pb_{1-x}Sn_xSe$ [48] and the V–VI compounds [49].

TABLE I. Bader charge analysis on different Sn-Se compounds at 10 GPa. Because of the very similar Bader charges of the nonequivalent Sn or Se atoms in $SnSe_2$, only the average values are shown.

	Sn (e)	Se (e)
SnSe	0.82	−0.82
Sn_3Se_4	0.94	−0.70
$SnSe_2$	1.15	−0.58

In summary, we have performed systematic variable-composition evolutionary searches in the tin-selenium system under hydrostatic pressures up to 40 GPa. A new cubic compound Sn_3Se_4 with an unusual stoichiometry is predicted to be stable above 10 GPa. Compared to the layered crystal structures of SnSe and $SnSe_2$, Sn_3Se_4 is more densely packed. Our calculations have been verified by the successful synthesis of Sn_3Se_4 in a diamond anvil cell. From synchrotron x-ray diffraction, the space group and the lattice constant are determined and they are in agreement with our theoretical results. Electronic structure calculations show that the new Sn_3Se_4 compound exhibits a metallic behavior, in sharp contrast to existing Sn-Se semiconductors. It is predicted that the metallization of Sn_3Se_4 leads to a superconducting transition at much lower pressures than previously expected for the Sn-Se binary system. Electron density and Bader charge analysis have been carried out to explore the mixed characters of the chemical bonding in Sn_3Se_4. This work suggests that new compounds with unexpected stoichiometries may exist in the IV–VI groups; novel and interesting properties may be sought within these unusual compounds.

We are grateful for the financial support from the Early Career Scheme of RGC under Project No. 27202516 and the research computing facilities offered by Information Technology Services, The University of Hong Kong. The experimental work is supported by NSAF (Grant No. U1530402) and NSFC (Grant No. 21501162). The authors are grateful for Dr. Yue Meng's support for laser heating experiments at HPCAT. HPCAT (Geophysical Lab) operations are supported by DOE-NNSA under Award No. DE-NA0001974 and DOE-BES under Award No. DE-FG02-99ER45775, with partial instrumentation funding by NSF. Advanced Photon Source is supported by DOE-BES, under Contract No. DE-AC02-06CH11357.

*likuo@hpstar.ac.cn
†yuechen@hku.hk

[1] D. Martínez-Escobar, M. Ramachandran, A. Sánchez-Juárez, and J. S. N. Rios, Thin Solid Films **535**, 390 (2013).

[2] Z. V. Borges, C. M. Poffo, J. C. de Lima, D. M. Trichês, T. P. O. Nogueira, L. Manzato, and R. S. de Biasi, Mater. Chem. Phys. **169**, 47 (2016).
[3] K.-M. Chung, D. Wamwangi, M. Woda, M. Wuttig, and W. Bensch, J. Appl. Phys. **103**, 083523 (2008).
[4] L.-D. Zhao, S.-H. Lo, Y. Zhang, H. Sun, G. Tan, C. Uher, C. Wolverton, V. P. Dravid, and M. G. Kanatzidis, Nature (London) **508**, 373 (2014).
[5] L.-D. Zhao *et al.*, Science **351**, 141 (2016).
[6] I. Loa, R. Husband, R. Downie, S. Popuri, and J. Bos, J. Phys. Condens. Matter **27**, 072202 (2015).
[7] Y. A. Timofeev, B. Vinogradov, and V. Begoulev, Phys. Solid State **39**, 207 (1997).
[8] M. Micoulaut, W. Wełnic, and M. Wuttig, Phys. Rev. B **78**, 224209 (2008).
[9] N. D. Boscher, C. J. Carmalt, R. G. Palgrave, and I. P. Parkin, Thin Solid Films **516**, 4750 (2008).
[10] T. Minagawa, J. Phys. Soc. Jpn. **49**, 2317 (1980).
[11] D. Bletskan, J. Ovonic Res. **1**, 47 (2005).
[12] K. Kirshenbaum, P. S. Syers, A. P. Hope, N. P. Butch, J. R. Jeffries, S. T. Weir, J. J. Hamlin, M. B. Maple, Y. K. Vohra, and J. Paglione, Phys. Rev. Lett. **111**, 087001 (2013).
[13] T. Chattopadhyay, A. Werner, H. Von Schnering, and J. Pannetier, Revue de Physique Appliquée **19**, 807 (1984).
[14] A. R. Oganov and C. W. Glass, J. Chem. Phys. **124**, 244704 (2006).
[15] A. R. Oganov, Y. Ma, A. O. Lyakhov, M. Valle, and C. Gatti, Rev. Mineral. Geochem. **71**, 271 (2010).
[16] Y. Chen, Q.-M. Hu, and R. Yang, Phys. Rev. Lett. **109**, 157004 (2012).
[17] A. J. Mannix *et al.*, Science **350**, 1513 (2015).
[18] Y.-L. Li, S.-N. Wang, A. R. Oganov, H. Gou, J. S. Smith, and T. A. Strobel, Nat. Commun. **6** 6974 (2015).
[19] J. Li and C. Fan, Phys. Chem. Chem. Phys. **17**, 1180 (2015).
[20] W. Zhang, A. R. Oganov, A. F. Goncharov, Q. Zhu, S. E. Boulfelfel, A. O. Lyakhov, E. Stavrou, M. Somayazulu, V. B. Prakapenka, and Z. Konôpková, Science **342**, 1502 (2013).
[21] A. Drozdov, M. Eremets, I. Troyan, V. Ksenofontov, and S. Shylin, Nature (London) **525**, 73 (2015).
[22] D. Duan, Y. Liu, F. Tian, D. Li, X. Huang, Z. Zhao, H. Yu, B. Liu, W. Tian, and T. Cui, Scientific reports **4**, 6968 (2014).
[23] D. Duan, X. Huang, F. Tian, D. Li, H. Yu, Y. Liu, Y. Ma, B. Liu, and T. Cui, Phys. Rev. B **91**, 180502 (2015).
[24] The projector-augmented wave method (PAW) [25] combined with the generalized gradient approximation (GGA) in the Perdew-Burke and Ernzerhof (PBE) form [26] was applied in all DFT calculations using VASP [27]. A cutoff energy of 350 eV was used for expanding the wave functions. Brillouin zone was sampled adopting the Γ-centered Monkhorst-Pack method with a density of about $2\pi \times 0.04$ Å^{-1}. The convergence criterion for electronic self-consistent calculation was 10^{-6} eV.
[25] P. E. Blöchl, Phys. Rev. B **50**, 17953 (1994).
[26] J. P. Perdew, K. Burke, and M. Ernzerhof, Phys. Rev. Lett. **77**, 3865 (1996).
[27] G. Kresse and J. Furthmüller, Comput. Mater. Sci. **6**, 15 (1996).
[28] The variable-composition evolutionary search was performed using USPEX [29]. New crystal structures were generated using the following schemes: heredity (40%), random (20%), softmutation/coormutation (20%), and transmutation (20%).
[29] A. O. Lyakhov, A. R. Oganov, and M. Valle, Crystal structure prediction using evolutionary approach, in *Modern Methods of Crystal Structure Prediction*, edited by A. R. Oganov (Wiley-VCH, Berlin, 2010), pp. 147–180.
[30] H. Mao, J.-A. Xu, and P. Bell, J. Geophys. Res. **91**, 4673 (1986).
[31] C. Prescher and V. B. Prakapenka, High Press. Res. **35**, 223 (2015).
[32] F. Holtzberg and S. Methfessel, J. Appl. Phys. **37**, 1433 (1966).
[33] A. Zerr, G. Miehe, and R. Riedel, Nat. Mater. **2**, 185 (2003).
[34] D. M. Teter and R. J. Hemley, Science **271**, 53 (1996).
[35] F. Holtzberg, T. McGuire, S. Methfessel, and J. Suits, J. Appl. Phys. **35**, 1033 (1964).
[36] R. Viennois, K. Niedziolka, and P. Jund, Phys. Rev. B **88**, 174302 (2013).
[37] Phonon dispersions were computed using the small displacement method implemented in Phonopy [38]. A $2 \times 2 \times 2$ supercell containing 112 atoms was used. For accurate atomic forces, the convergence criterion for electronic self-consistent calculations was increased to 10^{-8} eV.
[38] A. Togo, F. Oba, and I. Tanaka, Phys. Rev. B **78**, 134106 (2008).
[39] F. Tran and P. Blaha, Phys. Rev. Lett. **102**, 226401 (2009).
[40] H. Yu, S. Dai, and Y. Chen, Scientific reports **6** 26193 (2016).
[41] L. Makinistian and E. Albanesi, Comput. Mater. Sci. **50**, 2872 (2011).
[42] See Supplemental Material at http://link.aps.org/supplemental/10.1103/PhysRevLett.118.137002 for electron-phonon coupling calculations and Eliashberg function, which includes Refs. [43–45].
[43] P. Giannozzi, J. Phys. Condens. Matter **21**, 395502 (2009).
[44] N. Troullier and J. L. Martins, Phys. Rev. B **43**, 1993 (1991).
[45] P. B. Allen and R. Dynes, Phys. Rev. B **12**, 905 (1975).
[46] W. Tang, E. Sanville, and G. Henkelman, J. Phys. Condens. Matter **21**, 084204 (2009).
[47] C. W. Li, J. Hong, A. F. May, D. Bansal, S. Chi, T. Hong, G. Ehlers, and O. Delaire, Nat. Phys. **11** 1063 (2015).
[48] G. Shu, S. Liou, S. Karna, R. Sankar, M. Hayashi, M.-W. Chu, and F. Chou, Appl. Phys. Lett. **106**, 122101 (2015).
[49] G. Liu, L. Zhu, Y. Ma, C. Lin, J. Liu, and Y. Ma, J. Phys. Chem. C **117**, 10045 (2013).